THE ASTROPHYSICAL JOURNAL, 599:92–104, 2003 December 10

HUBBLE SPACE TELESCOPE IMAGES OF SUBMILLIMETER SOURCES: LARGE IRREGULAR GALAXIES AT HIGH REDSHIFT

S. C. CHAPMAN,[1] R. WINDHORST,[2] S. ODEWAHN,[2] H. YAN,[2] AND C. CONSELICE,[1]
Received 2003 April 30; accepted 2003 August 16

ABSTRACT

We present new *Hubble Space Telescope* Space Telescope Imaging Spectrograph (STIS) high-resolution optical imaging of a sample of 13 submillimeter luminous galaxies for which the optical emission has been pinpointed either through radio 1.4 GHz or millimeter interferometry. We find a predominance of irregular and complex morphologies in the sample, suggesting that mergers are likely common for submillimeter galaxies. The component separations in these objects are on average a factor 2 larger than in local galaxies with similarly high bolometric luminosities. The sizes and star formation rates of the submillimeter galaxies are consistent with the *maximal* star formation rate densities of 20 $M_{\odot}$ kpc^{-2} in local starburst galaxies (Lehnert & Heckman). We derive quantitative morphological information for optical galaxies hosting submillimeter emission: total and isophotal magnitudes, Petrosian radius, effective radius, concentration, aspect ratio, surface brightness, and asymmetry. We compare these morphological indexes with those of other galaxies lying within the same STIS images. Most strikingly, we find ~70% of the submillimeter galaxies to be extraordinarily large and elongated relative to the field population, regardless of optical magnitude. Comparison of the submillimeter galaxy morphologies with those of optically selected galaxies at $z \sim 2$–3 reveals the submillimeter galaxies to be a morphologically distinct population, with generally larger sizes, higher concentrations, and more prevalent major-merger configurations.

Subject headings: cosmology: observations — galaxies: evolution — galaxies: formation — galaxies: high-redshift — galaxies: starburst

1. INTRODUCTION

Submillimeter galaxies (Smail, Ivison, & Blain 1997) are candidates for the progenitors to massive spheroids in the local universe (e.g., Lilly et al. 1999). Their luminosities ($>10^{12}$ $L_{\odot}$) imply star formation rates (SFRs) large enough to build $\gg M^*$ galaxies in much less than a gigayear, while their volume density (Barger, Cowie, & Sanders 1999; Chapman et al. 2003c) is comparable to that of giant elliptical galaxies locally. However, it is not at all clear that submillimeter galaxies do in fact build giant elliptical galaxies. The timescales for the huge luminosities could be very short (e.g., Blain et al. 1999; Smail et al. 2002), consistent with galaxies with lower masses than the giant elliptical galaxies. Tacconi et al. (2002) have shown evidence that local galaxies of comparable luminosities to submillimeter galaxies (ultraluminous infrared galaxies, ULIRGs) cannot evolve into giant elliptical galaxies. The merger of two gas-rich disks in a system of even modest mass could lead to the generation of a brief period of great luminosity (Mihos & Hernquist 1996). Submillimeter galaxy selection is susceptible to picking out the most luminous bursts at any epoch. However, detection of CO molecular gas in five submillimeter galaxies (Frayer et al. 1998, 1999; Neri et al. 2003) and a claimed strong clustering from a spectroscopic study of the submillimeter population (Blain et al. 2003) are suggestive of massive systems for at least a fraction of the submillimeter galaxies. Locally, the most luminous objects are the ULIRGs, which show evidence of being driven by mergers (Mihos & Bothun 1998).

If the submillimeter sources are snapshots of galaxies in the process of formation, their optical morphologies should reveal the mergers in process. However, an ongoing difficulty with both the identification of the submillimeter galaxies (large submillimeter beam sizes and thus positional uncertainties) and the intrinsic faintness of most of the sources at optical wavelengths has impeded a detailed morphological study of the population (Smail et al. 1998). The identification hurdle was overcome for the majority of the submillimeter population by using the deepest radio surveys (rms noise as low as 4 μJy at 1.4 GHz; Richards 2000; Ivison et al. 2002; E. Fomalont et al. 2004, in preparation) to pinpoint the submillimeter emission through a high-redshift extrapolation of the far-IR/radio correlation (e.g., Helou et al. 1985; Condon 1992). The faint microjansky radio source population is dominated by star-forming galaxies and low-luminosity active galactic nuclei (AGNs), distant analogs of local luminous infrared galaxies, with suggested star formation rates of 10–1000 $M_{\odot}$ yr^{-1} (Windhorst et al. 1995; Richards et al. 1999). The submillimeter galaxies constitute a subset of the faint radio population, with 65% of submillimeter galaxies showing radio detections to 30 μJy at 1.4 GHz (Barger, Cowie, & Richards 2000; Chapman et al. 2001b, 2003a; Ivison et al. 2002).

The optical morphologies of the submillimeter galaxies have been difficult to study at high resolution, owing in part to the difficulty of obtaining deep *Hubble Space Telescope* (*HST*) images over wide areas ($S_{850\,\mu m} > 5$ mJy submillimeter galaxies number 500 deg^{-2}). The few submillimeter galaxies with *HST* observations (Smail et al. 1998; Ivison et al. 2001; Chapman et al. 2002b, 2002c; Sato et al. 2002) show a range in morphologies, with many apparently multicomponent systems suggestive of the *early stage mergers*, seen in ~25% of the local ULIRGs (Goldader et al.

[1] California Institute of Technology, MS 320-47, Pasadena, CA 91125.
[2] Arizona State University, Department of Physics and Astronomy, Tempe, AZ 85287-1504.

2002; Surace & Sanders 2000). In general, local luminous galaxies appear to encompass a luminosity-dependent morphology relation, from less disturbed to major-merger morphologies (Kim et al. 1998; Kim & Sanders 1998; Goldader et al. 2002) as luminosity increases, with the most luminous ($>10^{13}$ $L_{\odot}$) often dominated by quasi-stellar objects (QSOs) (Farrah et al. 2002). However, without a statistical sample of submillimeter galaxies with *HST* resolution, it is difficult to assess how the submillimeter galaxies relate to local luminous galaxies detected with *IRAS*. In this paper, we present a morphological analysis of a sample of radio-identified submillimeter galaxies using new deep *HST* Space Telescope Imaging Spectrograph (STIS) observations in the rest-frame UV. We discuss the sample selection and observations (§ 2), analyze the submillimeter galaxies relative to the general field population and the optically selected $z \sim 3$ galaxies (§ 3), and finally discuss the generally peculiar morphologies found for the submillimeter galaxies (§ 4).

2. SAMPLE AND OBSERVATIONS

We assembled a sample of 13 submillimeter galaxies lying in four distinct fields (the Hubble Deep Field [HDF], SSA 13, SSA 22, and the Westphal 14 hr field) for follow-up with *HST*. The submillimeter galaxies were detected with the Submillimeter Common-User Bolometric Array (SCUBA) on the James Clerk Maxwell Telescope and pinpointed within ground-based optical images using radio, X-ray, or millimeter interferometric identifications. These submillimeter sources were first presented in Barger et al. (1999, 2000) and Chapman et al. (2000, 2001a, 2001b, 2002a, 2002b). Details of each source and its identification at multiple wavelengths are presented in the Appendix. All submillimeter galaxies are brighter than $S_{850\ \mu m} > 4$ mJy, implying far-infrared luminosities greater than $10^{12.5}$ $L_{\odot}$ if they lie at $z > 1$. Eleven out of 13 sources have associated radio emission ($>5\ \sigma \times$ rms), with X-ray emission serving as secondary positional identifier.

These galaxy candidates were chosen from the catalogs in each field to uniformly sample the I magnitude distribution of the total radio-submillimeter galaxy population. In Figure 1, we plot the I magnitude distributions of the parent sample and the *HST* sample. The sources lie in the range $I = 21$–26 mag. We have presented measurements for I-band fluxes if the significance is 3 σ or higher; otherwise, we have represented the nonidentification of the submillimeter/radio source by the 2 σ limit of the optical image. Optical magnitudes were measured using the SExtractor program (Bertin & Arnouts 1996), from our own imagery as well as from imagery taken from the archives using Westphal-14, William Herschel Telescope, $I(5\ \sigma) = 25.2$ (point-source limit); SSA 22, CFHT-12K, $I(5\ \sigma) = 26.4$ (point-source limit); HDF, Subaru/SUPRIME (Capak et al. 2003); and SA 13, KPNO/MOSAIC and Subaru/SUPRIME archival imagery, $I(5\ \sigma) = 26.1$. Ground-based I magnitudes are measured in a 3″ aperture centered on the radio position. No reference was made in the selection to the ground-based optical imagery beyond the magnitude measurements, and the sample should be unbiased with respect to morphology.

HST imaging for this sample was obtained through a Cycle 10 program with the STIS to study the morphologies of the submillimeter luminous galaxies. Between 1 and 3 orbits of integration time (tailored to the ground-based magnitudes), giving 2340–7280 s of LOW SKY observation, were split between two exposures per orbit, using the 50CCD clear filter. The pipeline-processed frames were calibrated and aligned and cosmic-ray rejected using standard IRAF/STSDAS routines. The pixel size in the STIS images is 0.″0508. The 50CCD clear filter is roughly a Gaussian with 1840 Å half-width and a pivot wavelength of 5733 Å; we refer to the associated AB magnitude as $R'(573)$. The sensitivity limit reached is $R'(573) \sim 27.1$–27.6 mag (5 σ), corresponding to $R \sim 27.6$–28.1 mag for a point source with an Sb galaxy spectral energy distribution. The STIS images are presented in Figure 2, with radio centroids marked with a cross. All sources except one (SMM J131235.2) were significantly detected by STIS.

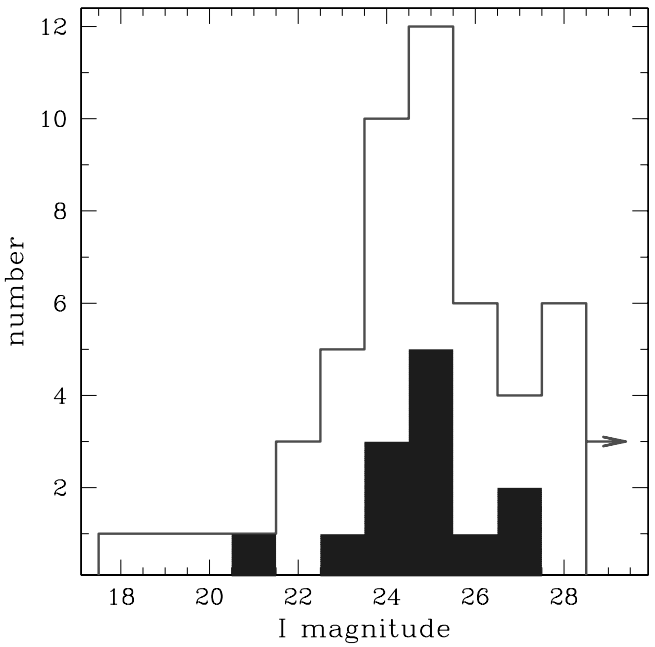

FIG. 1.—*I*-band magnitude distributions of the parent sample of submillimeter galaxies identified through their radio distribution (*line histogram*; Chapman et al. 2003a), compared with the *I* magnitudes of the *HST* sample considered here (*shaded histogram*). The faintest bin of the parent sample represents mostly lower limits to the *I*-band flux. The *HST* sources appear representative of the parent distribution.

The astrometry in the small (50″) *HST*-STIS images was fixed by smoothing the STIS image to the ground-based *I*-band resolution, matching all sources greater than 5 σ, and then transforming coordinate grids using the IRAF task GEOTRAN. After maximizing the cross-correlation signal between frames, the match between $I < 25$ optical sources has ±0.″1 rms. Since the large *I*-band mosaicked CCD images are precisely aligned (∼0.″3 rms) to the radio grid (e.g., Richards et al. 1999), the *HST* images should be aligned to the radio frame to ∼0.″3 rms.

While ground-based optical imaging with ∼1″ seeing typically identified only hints of extended sources, our STIS imaging uncovers complex morphologies and distinct components with intervening low surface brightness (SB) emission. While only two of our sources currently have spectroscopic redshifts, there are now over 50 robust measurements of field radio to submillimeter sources with $\langle z \rangle = 2.4$ and an interquartile range of $1.8 < z < 2.8$ (Chapman et al. 2003a; S. Chapman 2004, in preparation), suggesting that our *HST* targets should sample a similar

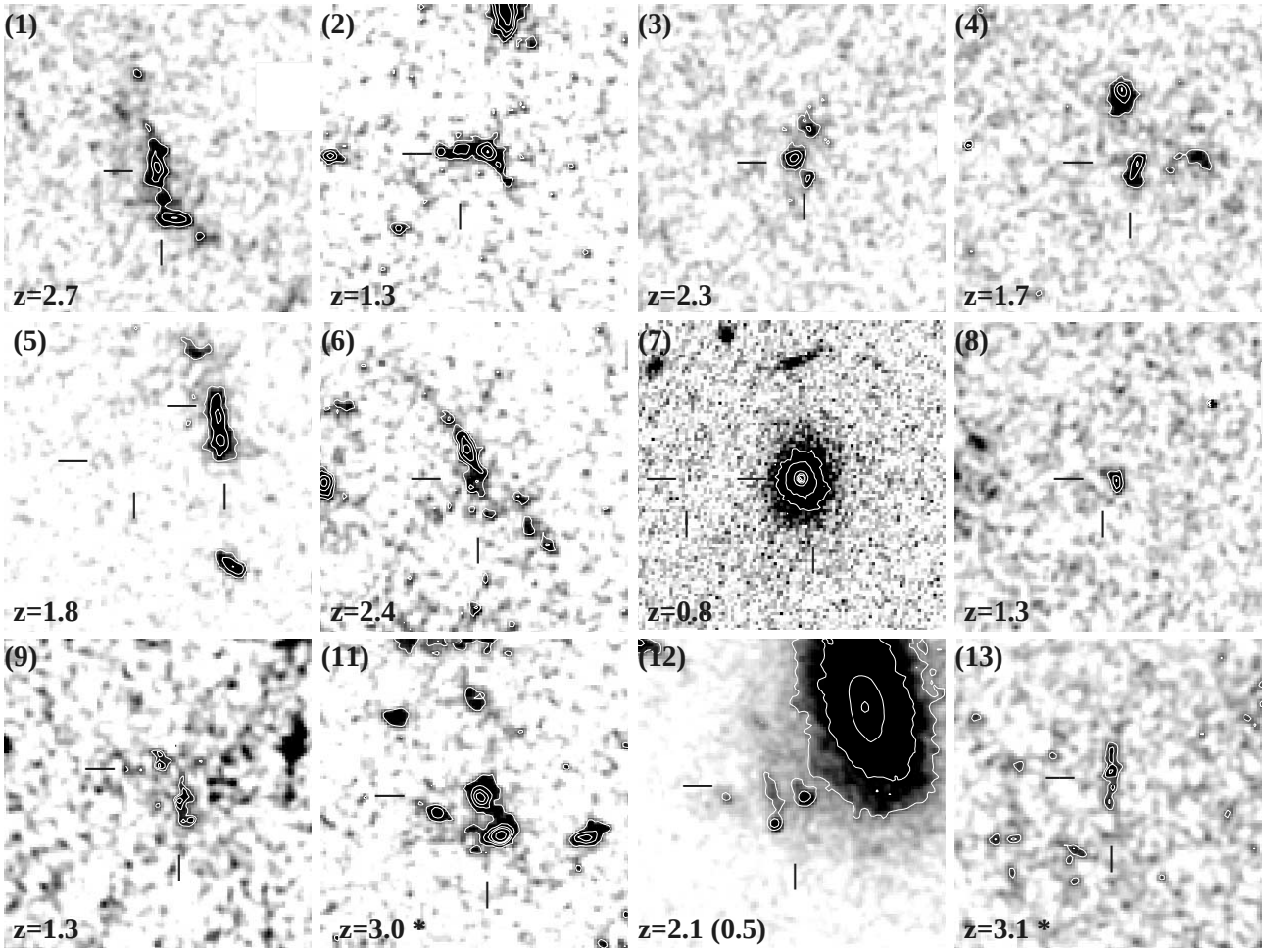

FIG. 2.—*HST*-STIS observations of submillimeter galaxies (6″ fields). Radio centroids are indicated with crosshairs. Redshifts are photometric (submillimeter/radio; Carilli & Yun 1999, 2000) except as indicated with an asterisk (spectroscopic) or in brackets (the redshift of the nearby elliptical). All images except source 7 have been smoothed with a Gaussian FWHM 0.″05 for better visibility.

redshift range. These measurements have confirmed that the submillimeter/radio redshift indicator (Carilli & Yun 1999) has large (∼50% rms) error, negating their use for studying optical luminosities. However, the angular diameter distance varies slowly over the redshift range $z = 1$–4, and the Carilli & Yun (1999) indicator is sufficient to assume a physical scale for their angular diameters (the submillimeter/radio ratio indicates redshifts for our sources lying between $z = 1.3$ and 3.1; see Fig. 2). All calculations assume a flat ΛCDM cosmology with $\Omega_\Lambda = 0.7$ and $H_0 = 65$ km s^{-1} Mpc^{-1}, so that 1″ corresponds to 8.6 kpc at $z = 1$, 9.0 kpc at $z = 2$, 8.3 kpc at $z = 3$, and 7.5 kpc at $z = 4$.

2.1. *Archival Images of Lyman Break Galaxies and Narrowband Galaxies*

In order to construct a morphological comparison sample of high-redshift galaxies, we obtained *HST*-Wide Field Planetary Camera 2 (WFPC2) images from the Canadian Astrophysics Data Center (CADC). We concentrate on Lyman break galaxies (LBGs; Steidel et al. 2003): rest-frame UV selected star-forming galaxies at $z \sim 2.5$–3.5. We also study Lyα emitters at $z \sim 3.1$, detected using a 80 Å narrowband filter (similar to that presented in Steidel et al. 2000), which we denote NB galaxies.

WFPC2 images in the F814W filter were obtained for literature LBG fields with at least 3 orbits of integration. These fields include the 0000−263 and 0347−383 fields originally presented in Giavalisco, Steidel, & Machetto (1996) and the SSA 22 field from Steidel et al. (1998). In addition, parallel WFPC2 exposures from our own primary STIS program in the SSA 22 field were used for this analysis. All NB galaxies lie in the SSA 22 field. The WFPC2 images have a pixel scale of 0.″1 and typically reach $I = 25.5$ at 5 σ, depending on the precise exposure time in the particular image.

We also use morphological parameters extracted for LBGs in the HDF, taken in the F606W filter. Details of these measurements can be found in Conselice et al. (2003b).

3. RESULTS

3.1. *Submillimeter Galaxies: General Morphology*

We begin our analysis of the submillimeter galaxy morphologies with a general assessment of their properties. Figure 2 shows the radio-identified optical components to the submillimeter sources, the photometric redshift (or spectroscopic redshift when available), and identifies the image with Table 1. The images in Figure 2 have been

TABLE 1

PHOTOMETRY AND MORPHOLOGY INDEXES FOR THE SUBMILLIMETER GALAXIES

Source	$S_{850\ \mu m}$ (mJy)	$S_{1.4\ GHz}$ (μJy)	I[a] (mag)	$R'(573)$[b] (mag)	R_{50}[c] (arcsec)	C32[d]	b/a[e]	b/a[f]	SB[g] (mag arcsec^{-1})	Size[h] (arcsec)
SMM J123553.3+621338.....	8.8 ± 2.1	58.4 ± 9.0	24.84	25.48	0.50	1.32	0.32	0.60	24.80	0.5
SMM J123600.1+620254.....	6.9 ± 2.0	262 ± 17	24.67	26.04	0.34	1.39	0.62	0.34	25.19	0.6
SMM J123616.2+621514.....	5.8 ± 1.1	53.9 ± 8.4	24.46	26.70	0.41	1.42	0.59	0.71	26.24	0.3
SMM J123618.3+621551.....	7.8 ± 1.6	151 ± 11	24.98	26.66	0.14	1.51	0.88	0.52	24.31	0.4
SMM J123621.3+621708.....	7.5 ± 2.3	148 ± 11.0	23.42	26.70	0.19	1.41	0.42	0.53	24.16	0.3
SMM J123622.7+621630.....	7.1 ± 1.7	70.9 ± 8.7	24.32	25.27	0.36	1.38	0.42	0.58	24.32	0.5
SMM J123710.0+622649.....	7.4 ± 2.2	551 ± 31	21.15	22.43	0.50	1.48	0.63	0.59	23.43	0.7
SMM J123713.9+621827.....	15.7 ± 2.4	595 ± 31	26.80	27.19	0.17	1.58	1.00	0.72	25.30	0.2
SMM J131231.9+424430.....	3.8 ± 0.8	127 ± 7.0	25.36	27.00	0.36	1.23	0.86	0.69	26.70	0.3
SMM J131235.2+424424.....	3.9 ± 0.9	34.1 ± 7.1	26.05	28.03	...	...	...	...	...	...
SMM J141809.8+522205.....	5.4 ± 1.4	<58	24.57	24.14	0.38	1.19	0.70	0.73	23.75	0.6
SMM J221724.7+001242.....	13.2 ± 3.0	120 ± 34.0	25.21	25.78	0.37	1.38	0.35	0.75	24.47	0.6
SMM J221726.1+001239.....	17.8 ± 2.3	<53	26.11	26.82	0.38	1.47	0.41	0.27	25.76	0.3

[a] Ground-based I magnitude in 3″ aperture centered on radio position.
[b] *HST* magnitude down to 1.5 σ ellipse isophote.
[c] Effective radius, down to 50% light contour.
[d] Concentration index.
[e] b/a from intensity-weighted moment.
[f] b/a from least-squares fit of an ellipse out to the 1.5 σ SB isophotal contour.
[g] Mean surface brightness (SB; magnitudes per arcsec^2) within the effective radius.
[h] Image size (in arcseconds) from the intensity-weighted image moment.

smoothed with contours overlaid to increase the visibility of faint structures in the submillimeter galaxies. For an unsmoothed version of this figure, see the companion paper (Conselice, Chapman, & Windhorst 2003a). Descriptions of the individual objects in the sample can be found in the Appendix.

Inspection of the images in Figure 2 reveals that many of the submillimeter galaxies display a distinct extended, linear morphology. A brighter knot is often asymmetrically displaced toward the end of a linear, lower surface brightness nebulosity surrounding the compact components. Multiple components are often revealed within $\sim$1″–2″ scales. A few of the submillimeter galaxies look similar to *chain* galaxies (Cowie, Hu, & Songaila 1995), while others are suggestive of mergers in progress, a statement that we will further quantify below.

Local infrared-luminous galaxies have been identified with merging galaxy morphologies (Sanders & Mirabel 1996). As a simple, illustrative comparison, the submillimeter galaxy component separations and elongations can be compared to the highest luminosity local galaxies: the ULIRG subset from the 1 Jy sample of *IRAS* galaxies from Veilleux, Kim, & Sanders (2002; see also Murphy et al. 1996). As shown in Figure 3, the distribution in component separation of local ULIRGs is peaked at small values but has a significant tail at higher values. These measurements consider components with nuclear magnitudes of $M_R < -20.1$. The trend in Veilleux et al. (2002) is for the highest luminosity ULIRGs (those with $L_{ir} > 3 \times 10^{12}\ L_\odot$) to have significantly smaller nuclear separations than the $1 \times 10^{12} < L_{ir} < 3 \times 10^{12}$ ULIRGs.

We place the submillimeter galaxies on the same plot by measuring the maximum extent between multiple component structures, centroiding on the outermost intensity peaks within coherent structures (those exhibiting low surface brightness bridges). The submillimeter galaxies by contrast all have projected separations of greater than 5 kpc, except for sources 7 and 8, which do not exhibit multiple component or extended structures. The submillimeter galaxy STIS images likely represent rest-frame wavelengths of 1500–3000 Å, and we must be cautious of direct comparison with the R-band local fiducial from Veilleux et al. (2002). Consideration of rest-frame UV images of ULIRGs

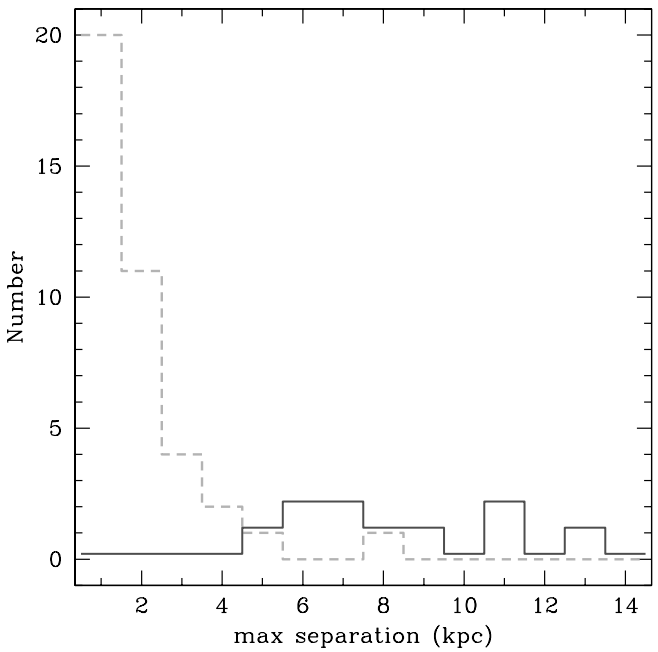

FIG. 3.—Apparent nuclear separations for the submillimeter galaxies (*solid line*) compared to the 1 Jy sample of *IRAS* galaxies from Veilleux et al. (2002; see also Murphy et al. 1996) (*dashed line*). The submillimeter histogram binning is twice as large as that for the *IRAS* sample. The distribution of local *IRAS* galaxies is highly peaked at small values but has a significant tail at higher values. The submillimeter galaxies all have separations of greater than 5 kpc except sources 7 and 8, which do not exhibit multiple component or extended structures.

(Goldader et al. 2002) suggests that UV-bright star clusters can become apparent within galactic nuclei but do not significantly affect the global separation measurements presented in Figure 3.

This result suggests that the merger configurations of high-redshift submillimeter galaxies are typically larger and at an earlier stage than those of comparable luminosities at low redshift identified in the infrared by *IRAS*.

3.2. *Submillimeter Galaxies: Quantitative Morphology*

In order to associate quantitative measures to these visual impressions of the submillimeter galaxies, we undertook a morphological analysis of the STIS images of submillimeter galaxies under the LMORPHO environment (Odewahn et al. 2002). Catalogs of all sources in each of the nine STIS fields were first prepared, covering an area 0.00161 deg^2. An initial SExtractor (Bertin & Arnouts 1996) catalog was assembled, computed with a 1 σ threshold, a fixed 5 pixel aperture, and a predetection smoothing Gaussian with $\sigma = 5$ pixels in a 9×9 pixel filter. A total of 619 sources were cataloged. An interactive editing tool was then used to perform star-galaxy separation and source-detection cleaning (i.e., fixing obvious mistakes in image segmentation by SExtractor or eliminating detected image defects, etc.), yielding 611 sources with photometry from the automated galaxy surface photometry package (GALPHOT). The submillimeter sources, along with the 102 galaxies with nearby companions ($<1''$), were isolated, and GALPHOT was rerun interactively to locate and eliminate nearby sources in the final photometry and to determine more reliable local sky values to improve the photometry.

The submillimeter optical counterparts are detected with sufficient signal-to-noise ratio (S/N) (>10 beam^{-1}) for detailed morphological analysis but are clearly much too faint for the application of a Fourier-based classifier (e.g., Odewahn et al. 2002). We estimate standard quantitative measures of galaxy morphology. Table 1 lists ground-based submillimeter, radio, and *I* magnitude photometry, along with these morphological parameters extracted from the *HST* images: total magnitude, effective radius R_{50}, concentration index, aspect ratio, image size, and mean surface brightness.

The CAS (concentration, asymmetry, and clumpiness) program for morphological analysis (Conselice 2003) was also employed to quantify the asymmetries of the submillimeter galaxies. CAS is based on the idea that structural and morphological features of galaxies are directly related to past and present underlying physical processes. The processes traced by CAS are the past and present star formation and merger activity. In the CAS system, the asymmetry index (A) is used to determine whether a galaxy is involved in a major merger (Conselice, Bershady, & Gallagher 2000; Conselice et al. 2003b; Conselice 2003). In this system major mergers are always found to have an asymmetry greater than some limit, which in the rest-frame optical is $A_{\rm merger} = 0.35$. The concentration index is also a fair representation of the scale of a galaxy and is proportional to the fraction of stars in a bulge component (e.g., Graham et al. 2001; Conselice 2003).

In a similar manner to the LMORPHO analysis, galaxies with nearby companions ($<1''$) were isolated before calculating morphological quantities. We placed our initial guess for the center on the brightest portion of the submillimeter galaxy and then ran the CAS program to determine the asymmetry and light concentrations for these galaxies. This is done through well-defined radii and centering and background removal methods, which are fully described in Conselice (2003). Morphological parameters extracted include asymmetry, concentration, and a growth-curve estimate of effective radius, or Petrosian radius (Bershady, Jangren, & Conselice 2000; Conselice et al. 2000), and are listed in Table 2. The Petrosian radius (in units of arcseconds) is defined as $1.5 \times r_{(\eta=0.2)}$, where $\eta = 0.2$ is the radius (r), where the surface brightness within an annulus at r is one-fifth the surface brightness within r. This provides a measure of size that does not depend on isophotes, complementary to that of the image moment based R_{50} from the LMORPHO analysis above. Corrections have been applied to the asymmetry and concentration values using an offset computed through the simulation to show how local normal galaxies would appear at the redshifts of submillimeter galaxies (Conselice et al. 2003a, a companion paper that provides detailed CAS analysis of the submillimeter galaxies and their merger fraction relative to other galaxy populations).

TABLE 2

CAS Morphology Indexes for the Submillimeter Galaxies

Source	Concentration	Asymmetry	$R_{\rm Petrosian}$ (arcsec)
SMM J123553.3+621338.....	3.26	0.14	2.09
SMM J123600.1+620254.....	3.47	0.10	1.39
SMM J123616.2+621514.....	3.91	0.47	1.23
SMM J123618.3+621551.....	3.73	0.35	1.20
SMM J123621.3+621708.....	3.92	0.05	4.05
SMM J123622.7+621630.....	3.43	0.05	2.61
SMM J123710.0+622649.....	3.93	0.12	0.72
SMM J123713.9+621827.....	3.87	0.11	0.71
SMM J131231.9+424430.....	2.01	0.16	1.05
SMM J131235.2+424424.....	N/A	N/A	N/A
SMM J141809.8+522205.....	3.02	1.05	0.73
SMM J221724.7+001242.....	3.01	0.23	7.63
SMM J221726.1+001239.....	2.12	0.39	0.84

3.3. *Comparison of the Submillimeter Galaxies with the Field Catalog*

Morphological analysis of faint sources can be susceptible to differences in the image depth, instrumental response, and pixel sampling (e.g., Odewahn et al. 2002). Therefore, the most direct approach to studying the morphologies of the submillimeter sources is to compare the photometric properties of the submillimeter/optical counterparts with the general population of optical sources in the same nine STIS frames. The results of this analysis are presented in Figure 4.

Figure 4*a* plots the isophotal effective radius (R_{50}) as a function of total magnitude. R_{50} is a measure of the deprojected radius containing 50% of the light represented by the total magnitude. Most of the submillimeter sources (eight of 11) exhibit larger effective radii ($R_{50} > 0.35$) per magnitude interval than the general population. In the STIS magnitude bin 25–27 (subsuming the submillimeter galaxies), the median $R_{50} = 0.18$, with an interquartile range 0.12–0.23. We emphasize that while sources with $z < 1$ cannot be directly compared with the submillimeter galaxies, they

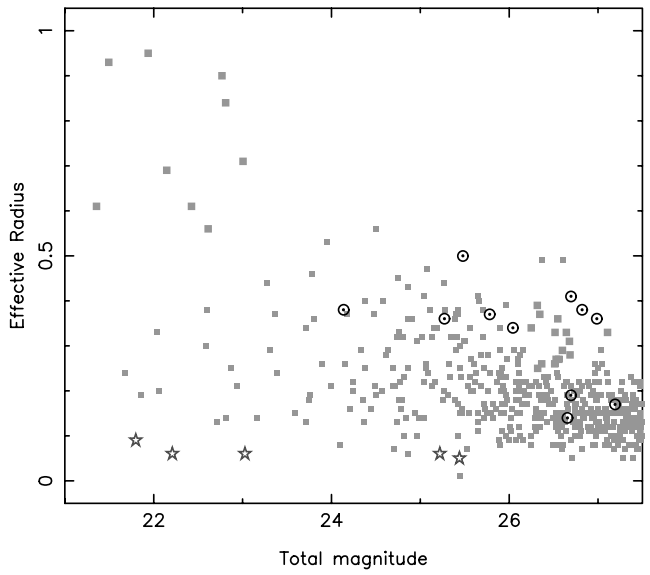

FIG. 4*a*

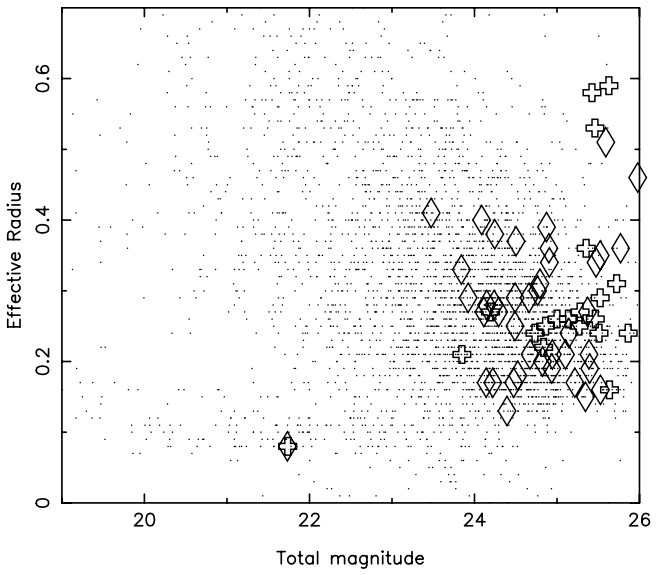

FIG. 4*b*

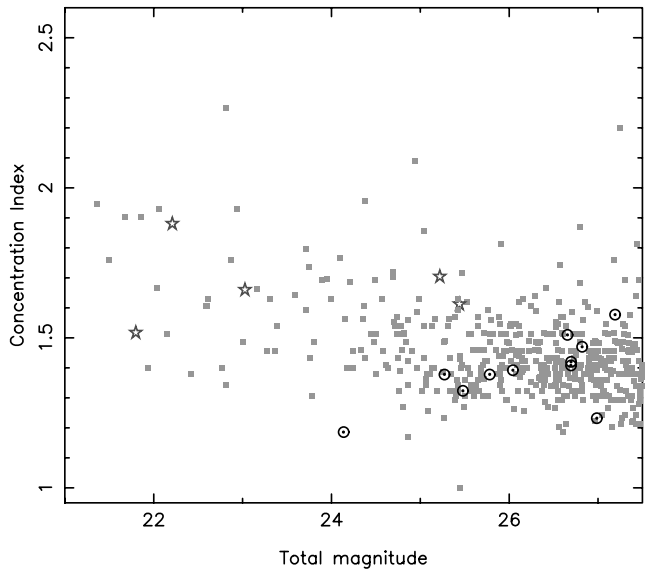

FIG. 4*c*

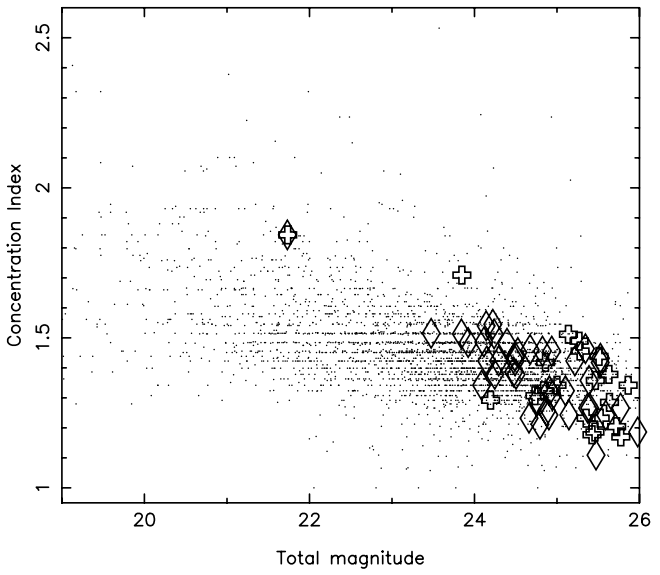

FIG. 4*d*

FIG. 4.—*HST*-STIS derived morphological parameters for the submillimeter galaxies (*left panels*). *Circles*: Submillimeter galaxies. *Squares*: Field galaxies. *Stars*: Stars. For comparison, we show the same parameters for the Lyman break galaxies (*diamonds*) and $z \sim 3.1$ narrowband Lyα galaxies (*crosses*) in the right panels. (*a–b*) Effective radius (R_{50}) as a function of total magnitude. (*c–d*) Concentration index (C32 = ratio of 75% to 25% quartile sizes) vs. magnitude. Higher C32 means more compact. (*e–f*) Mean surface brightness within the effective radius (magnitude arcmin^{-2}) vs. semimajor axis radius in arcseconds.

must exhibit smaller physical scales per unit angle, making the comparison with the extended submillimeter galaxies even more dramatic. Before attempting to interpret this result, it is important to consider how R_{50} is calculated. Each pixel is deprojected based on the isophotal ellipse shape and orientation in the usual manner, giving a measure of the pixel distance from center in the equatorial plane of the galaxy. These spatial measures are binned radially and used to compute the mean surface brightness. Integrating and extrapolating this profile produces a total magnitude and a growth curve. Using this growth curve we derive R_{50}, a measure of the deprojected radius at which 50% of the total light is collected. As galaxies become more edge-on, there are fewer sampled points to use for the deprojection in the semimajor axial direction. An infinitely thin, perfectly edge-on galaxy cannot have its R_{50} calculated in this manner. As a result, galaxies approaching this idealization can exhibit R_{50} values larger than physically represented. This systematic effect, combined with the highly elongated nature of our submillimeter galaxy images, causes the submillimeter galaxy points in Figure 4*a* to occupy the upper R_{50} envelope of the point distribution that is dominated primarily by *roundish* field galaxies.

The CAS estimate of the Petrosian radius provides a complementary analysis to the R_{50} result. The average Petrosian radius of the submillimeter galaxies ($2\farcs1$) is larger than any other star-forming galaxies at low or high redshift (after taking redshift effects into account; Conselice et al. 2000). Lyman break galaxies from the Hubble Deep Field have a Petrosian radius of $1\farcs2$ (Conselice et al. 2003b). The CAS

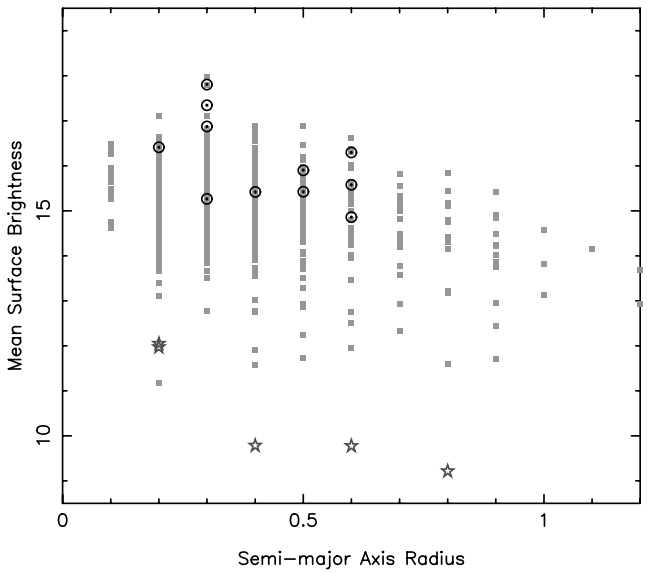

FIG. 4*e*

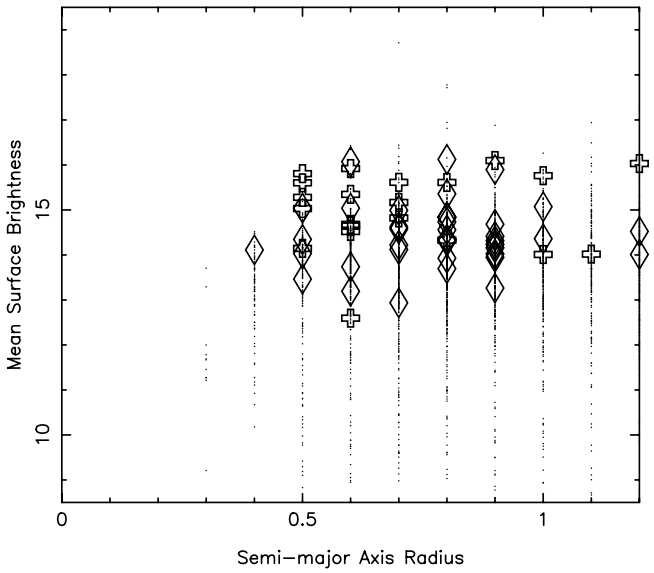

FIG. 4*f*

analysis thus supports our finding, using the R_{50} index, that submillimeter galaxies are larger systems than other star-forming galaxies. We have also verified our finding from the pair separation.

Analysis of the field galaxies exhibiting a similar range of R_{50} to the submillimeter galaxies reveals that they are split approximately in half between apparently large galaxies (likely to be nearby) and linear/edge-on galaxies. The latter are reminiscent of the submillimeter galaxy morphologies. There are 12 field galaxies within the magnitude range $R'(573) = 24$–27 (subsuming the magnitude range of the eight submillimeter galaxies with large R_{50}) having morphologies *similar* to those of the submillimeter galaxies. As we have targeted our STIS images around relatively bright (>5 mJy) and rare (0.25 arcmin^{-2}) submillimeter sources, we must scale by this value to calculate the total number of field galaxies with similar morphologies. This suggests that there are roughly 4 times the number of field galaxies with similar magnitudes and morphologies to the submillimeter galaxies but lacking the copious bolometric luminosities (the field galaxies are undetected in the submillimeter and radio images covering the same *HST*-STIS images).

Figure 4*b* shows concentration index (C32 = ratio of 75% to 25% quartile sizes) versus magnitude. Higher C32 implies a more compact light distribution (i.e., stars have large C32). We note that submillimeter sources follow an apparently opposite trend compared to the control sample. The mean C32 stays constant or increases slightly with fainter magnitude for the submillimeter sources but decreases slowly for the control galaxy sample. For the general population, we are simply seeing the effect of decreasing S/N and effective resolution as magnitudes become fainter: everything becomes diffuse (lower C32). The faint [$R'(573) > 26.5$] submillimeter sources have a higher C32 than the control sample, suggesting submillimeter selection picks out more concentrated galaxies.

Finally, Figure 4*c* shows the image size (in arcseconds) derived from the intensity-weighted image moment on the abscissa and the mean surface brightness (SB; magnitude per arcmin^2) within the effective radius on the ordinate. The data are discrete on the abscissa as image sizes are established in integral pixel units. The submillimeter sources are average or fainter in mean SB per size interval than the general population. We demonstrated above that submillimeter galaxies are more extended than the field galaxies (larger R_{50} and Petrosian radius and larger component separations than local infrared-luminous galaxies). The large, multi-component configurations tend toward low global SB measurements. Dust extinction, expected to be significant in submillimeter galaxies, will also make the rest-UV emission fainter. Surface brightness dimming at the high redshifts of the submillimeter galaxies $\propto(1+z)^4$ would also contribute to this trend.

While higher surface brightness core components are often present in the submillimeter galaxies, the average surface brightnesses (Fig. 4*c*) are not unusually high compared to the field STIS population. At ~25 mag arcsec^{-2} and redshifts with a median $z \sim 2.4$ (Chapman et al. 2003c), they correspond to about 10 times that observed in a typical spiral disk locally.

4. COMPARISON WITH LYMAN BREAK GALAXY MORPHOLOGIES

LBGs (Steidel et al. 1996, 1999) represent rest-frame UV selected star-forming galaxies at similar redshifts to submillimeter galaxies ($z \sim 2.5$–3.5). LBGs have *HST* morphologies that often exhibit distorted and irregular morphologies (Giavalisco et al. 1996; Steidel et al. 1996; Erb et al. 2003). However, there has never been a chance to compare against the submillimeter-selected galaxies. In Figure 5, we have reproduced a complete sample of LBGs from Steidel et al. (2003) using sources from the fields presented in Giavalisco et al. (1996) and Steidel et al. (2000), as described in § 2.1, with the goal of applying the same analyses as were performed on the submillimeter galaxies.

Another class of high-redshift galaxies are the Lyα emitters (e.g., Cowie & Hu 1998). These galaxies have been isolated at $z = 3.1$ using an 80 Å narrowband filter and compared to the LBG population in the same field (Steidel et al. 2000). We have recently obtained a much larger image of the same region in a similar filter (S. Chapman 2004, in

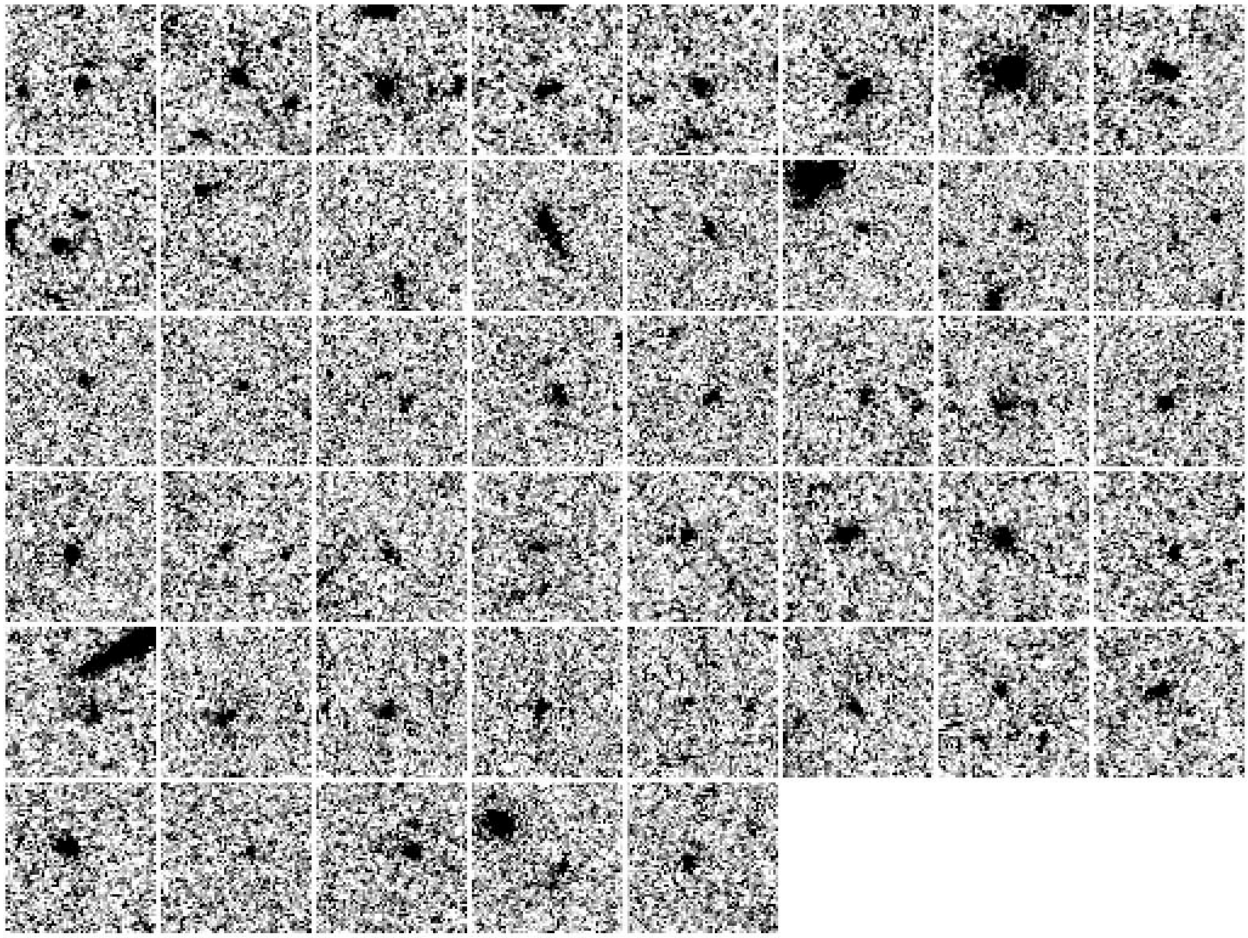

FIG. 5.—*HST*-WFPC2 observations of Lyman break galaxies (6″ fields). Galaxies will have redshifts lying within the LBG selection function of $z = 2.5$–3.5 (Steidel et al. 1999). The pixel size is 0.″1 for these images. As the sources are generally brighter than the submillimeter galaxies and the pixel scale is larger, the images have been left unsmoothed to preserve extended structure.

preparation). Steidel et al. (2000) have demonstrated that only 25% of LBGs satisfy the large equivalent widths in Lyα to be detectable in such narrowband (NB) images. In Figure 6 we show the *HST* images of all NB galaxies in the SSA 22 field, lying within the WFPC2 archival images. As these objects are generally much fainter than the LBGs, we have smoothed the images for visibility.

4.1. *Morphological Parameters*

To compare the LBGs and NB galaxies to the submillimeter galaxies in a self-consistent manner, we applied the same morphological analysis to the complete galaxy catalogs from the WFPC2 images using the same LMORPHO environment. This enables the same normalization against the field population as we used for the STIS images of submillimeter galaxies (§ 3.2), removing any instrumental biases. The effective radius in particular (Fig. 4*a*) suffers from large instrumental dependency because of the pixel scales of the images.

Figures 4*a* and 4*b* suggest that neither LBGs nor NB galaxies generally differentiate themselves from the field galaxy population, in either effective radius or concentration index. This is opposite the finding from § 3.2 for the submillimeter galaxies that show larger R_{50} and an opposite trend in concentration index than the field galaxies. There do appear to be several LBGs at the fainter end of the total magnitude scale that are identified as having larger effective radii. Inspection of these sources reveal them to be among the closest morphological matches to the submillimeter galaxies. We emphasize that the submillimeter galaxies and LBGs can only be compared explicitly to their respective field samples, and not to each other, because of the sensitivity of these parameters to the STIS and WFPC2 instruments.

Figure 4*c* reveals the LBGs to have surface brightnesses $\sim$1.3 mag higher than the submillimeter galaxies. The NB galaxies are comparable in surface brightness to the submillimeter galaxies. This reflects the trend for LBGs to be dominated by a central knot of high surface brightness surrounded by lower surface brightness nebulosity, as previously described in Steidel et al. (1996).

We can also study the CAS parameters of the submillimeter galaxies compared to LBGs (here the NB galaxies are not considered because of typically lower S/N). As discussed above, and in Conselice et al. (2003a), the CA values for the submillimeter galaxies and LBGs have been corrected by redshifting nearby galaxies to $z = 3$ and seeing how the average CA values change because of redshift effects. As mentioned above, the average size of the submillimeter galaxies are larger than the LBGs: 2.″1 (submillimeter) versus 1.″2 (LBGs). The submillimeter galaxies

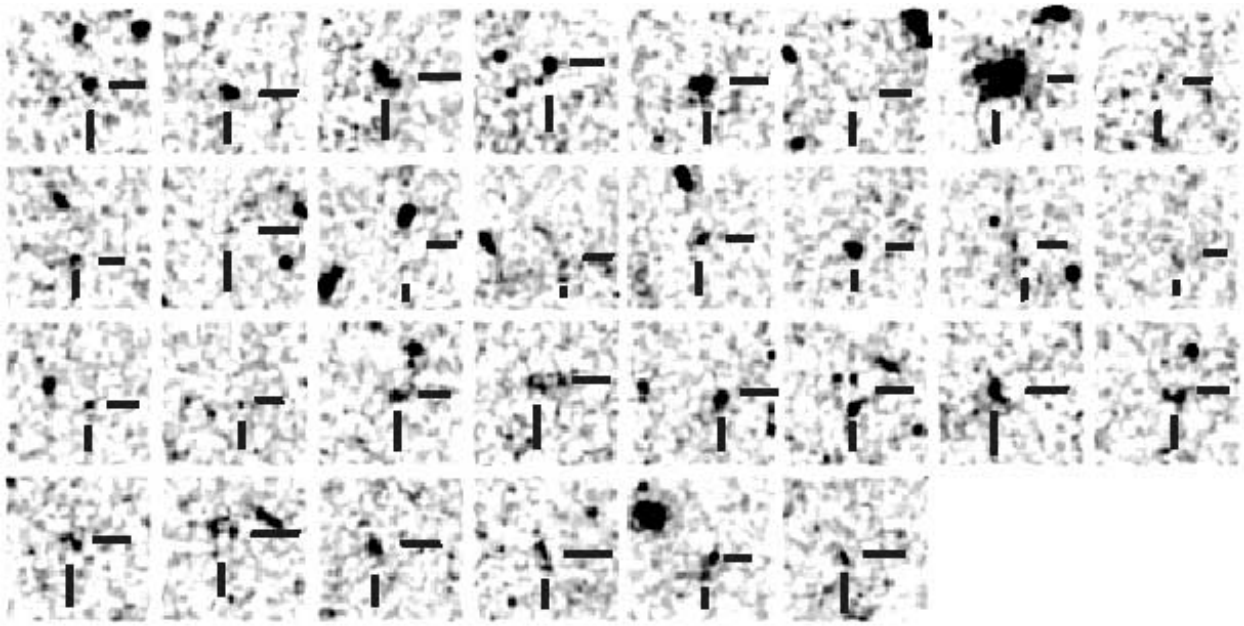

FIG. 6.—*HST*-WFPC2 observations of $z \sim 3.1$ sources selected as narrowband Lyα excess objects, as described in Steidel et al. (2000). Field size is 6″. As the narrowband galaxies are generally near the detection limit of the WFPC2 imagery, the images have been smoothed with a Gaussian FWHM 0.″05 for better visibility. The location of the narrowband source has been indicated with the crosshairs.

also distinguish themselves from the LBGs in terms of concentration but are similar in asymmetry. Figure 7 plots A and C for both LBGs and submillimeter galaxies, where the submillimeter galaxies have about the same asymmetry in the median but are more concentrated (3.2 vs. 2.1 for LBGs). This difference may reflect extended, bright starbursts or AGNs in the submillimeter galaxies.

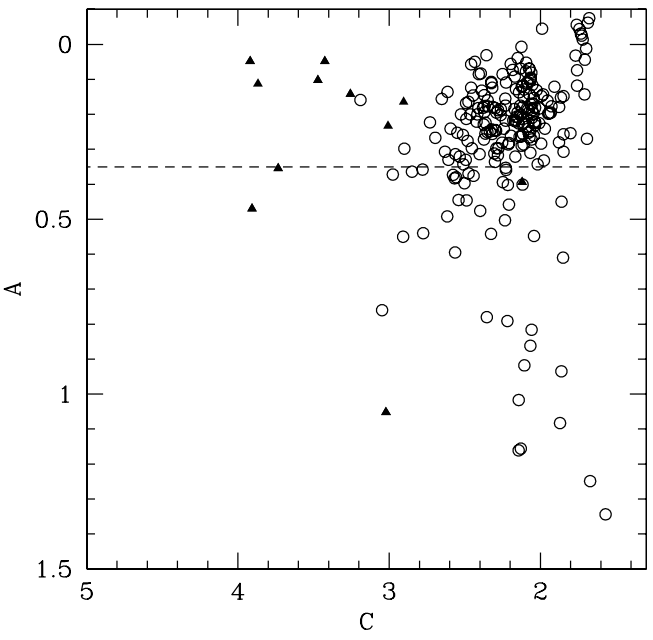

FIG. 7.—Plot of concentration index (C) and asymmetry (A) for both LBGs in the HDF from $z = 2$–3 (*circles*) and submillimeter galaxies (*triangles*). The submillimeter galaxies are significantly more concentrated than the LBGs. The asymmetries are similar for the submillimeter galaxies and LBGs.

4.2. *A Qualitative Classification Scheme*

Traditional quantitative measures of morphology have difficulty contending with the range of distorted, merger configurations exhibited by the submillimeter galaxy population. Subtle features of the morphologies can be missed by applying algorithmic processes to the inherently irregular light distributions. To complement our constraints on the quantitative morphological comparison of high-redshift galaxies, we devise a simple classification scheme to encompass the range of submillimeter galaxy morphologies, which distinguishes the main features seen in our *HST* images. The categories and memberships are listed in Table 3.

We delineate the following five categories: compact regular, compact irregular, elongated regular, elongated irregular, and multiple component/elongated irregular. These categories were applied independently to the submillimeter galaxies by members of our group, with the same results. The majority (83%) of the submillimeter galaxies are clearly in the latter two categories, with combinations of irregular, multiple components. Only two submillimeter galaxies (sources 7 and 8) can be considered isolated and compact (compact regular category).

We attempt to place the LBGs and NB galaxies within the same qualitative classification scheme that we applied to the submillimeter galaxies. We have used both the unsmoothed and smoothed images to study the morphologies for consistency with the submillimeter galaxies and in order not to miss faint extended structures.

One difficulty with the comparison is that the LBGs are typically optically brighter than the submillimeter galaxies, displaying high central surface brightness cores surrounded by lower surface brightness nebulosity (Steidel et al. 1996; Giavalisco et al. 1996; our Fig. 5). The submillimeter galaxies are generally lower surface brightness objects, with only bright cores rising above the noise level. However, we would expect this difference to produce a one-way bias, in

TABLE 3

QUALITATIVE CLASSIFICATIONS FOR SUBMILLIMETER GALAXIES, LBGS, AND NARROWBAND GALAXIES

Classification	Submillimeter Galaxies	LBGs	NB Galaxies
Compact regular	2 (17%)	20 (44%)	8 (27%)
Compact irregular	0 (0%)	15 (33%)	10 (33%)
Elongated regular	0 (8%)	2 (30%)	1 (3%)
Elongated irregular	3 (25%)	5 (11%)	8 (27%)
Irregular, multiple component	7 (58%)	3 (7%)	3 (10%)

the sense that the submillimeter galaxies should only appear less irregular because of loss in surface brightness sensitivity. By contrast, the NB galaxies are sometimes even fainter than many of the submillimeter galaxies, and even more structure may be lost in the noise.

The placement of the various LBGs into the categories outlined for the submillimeter galaxies is often challenging, whereby very faint sources neighboring more dominant central sources are often present. While these could be classified as "multiple component," they do not appear to represent the same type of major-merger configuration as the submillimeter galaxies (see also Conselice et al. 2003a). We have typically classified these sources as compact irregular, when the separations of the peaks are less than $0\farcs5$.

Compared with the LBGs, the submillimeter galaxies typically appear more extended with multiple components of larger separation, although both populations exhibit similar morphologies in a few of their representatives. The NB galaxies are more difficult to classify but also generally appear to be more compact than the submillimeter galaxies, although less so than the LBGs. The summary of this comparison is listed in Table 3.

5. DISCUSSION

Our *HST* images have identified the counterparts of submillimeter galaxies and allowed a quantification of their morphological properties. The galaxies are characterized by larger sizes than the field population in the same STIS images, confirmed by R_{50} and growth-curve estimates of the radii (Petrosian radii) compared to other populations. The isophotal R_{50} values provide a quantitative index that separates the peculiar morphologies of the submillimeter galaxies from the bulk of the field population. It also appears to differentiate the submillimeter galaxies from other high-redshift star-forming galaxies, the LBGs and NB galaxies, which generally do not distinguish themselves from the field population in the basic morphological parameters.

However, the R_{50} index does not fully describe the stunning morphologies of the submillimeter galaxies. Many show multiple components or extended structure beyond that extracted by the analysis routines. The morphologies appear to extend over scales conceivably up to $5''$ ($\sim$40 kpc), including regions beyond the radio emission, and therefore unlikely to be directly emitting the bulk of the bolometric luminosity. The separations of components in the submillimeter galaxies are typically larger than comparable luminosity systems in the local universe (Fig. 3). These morphologies are contrasted with the appearances of LBGs and NB galaxies, which are generally more compact. The comparably large asymmetries of submillimeter galaxies and LBGs relative to local normal galaxies indicates that LBGs are still highly irregular systems, although typically smaller.

The submillimeter galaxies typically have implied SFRs of $\sim$1000 $M_\odot$ yr^{-1} and total projected areal coverage of $\sim$50 kpc^2 traced in the rest-frame UV light from young stars observed by our STIS imagery (assuming the typical redshifts of the submillimeter galaxies; Chapman et al. 2003c). This corresponds to a SFR density of $\sim$20 $M_\odot$ yr^{-1} kpc^{-2}. Lehnert & Heckman (1996) have suggested that local star-forming galaxies are self-regulated by a *maximal starburst* of the same $\sim$20 $M_\odot$ yr^{-1} kpc^{-2} (for a Salpeter IMF). While the equality of the numbers is likely coincidental, the large sizes of the submillimeter galaxies are suggestive that starbursts of this order ($\sim$1000 $M_\odot$ yr^{-1}) cannot exist in smaller galaxies: contrast the smaller sizes and lower characteristic SFRs of the LBG population.

There is, however, no way to conclude from the present data whether an AGN may be responsible for some fraction of the bolometric luminosity. The resolved nature of submillimeter galaxy morphologies suggests that strong optical QSO components are not common in the submillimeter population. The large UV extent of the submillimeter galaxies may be evidence that star formation dominates the dust heating in many cases. Indeed, the only isolated source in our sample (SMM J123713.9) is also the smallest and most compact and is in fact the brightest *Chandra* X-ray source from our radio-identified submillimeter population in the HDF region, suggesting a dominant AGN (see also Alexander et al. 2003). This hypothesis is bolstered by the high spatial resolution radio measurements using the MERLIN radio interferometer ($\sim0\farcs3$ synthesized beam) of several sources from our *HST* sample (T. Muxlow 2004, in preparation). In $\sim$50% of the cases, the radio emission is extended and traces the UV morphology.

Can mergers truly produce a linear, elongated structure, reminiscent in some cases of *chain* galaxies (Cowie et al. 1995)? To address this question, we have studied the fraction of low-redshift ULIRG merger systems that look like linear, elongated structures. As described in Conselice et al. (2003a) *HST* images of low-z ULIRGs are redshifted to the submillimeter galaxy distances: 14 out of 51 (27 structures that look like chain galaxies. This is a comparable fraction to the submillimeter galaxy morphologies that also look like chain galaxies. Comparing with Cowie et al. (1996), the fraction could be argued to be even higher. We therefore consider $\sim$30% to be a conservative limit of the number of low-z ULIRGs that have morphologies consistent with the submillimeter galaxies.

The components of submillimeter galaxies may therefore represent the first generation of merging of substantial fragments of galaxies. The large fraction of highly elongated or linear structures (some similar to the chain galaxies of

Cowie et al. 1995) are suggestive of early stages of a dynamical event in which two approximately equal-mass clumps have passed by or through each other. If the components do not subsequently reach escape velocity, they will fall back into each other and become a merger in the near future. Such an initial dynamical event would induce star formation on the dynamical timescale for the system. Submillimeter galaxies may be hosted by very high mass halos, based on their strong redshift clustering (Blain et al. 2003). This is consistent with the CO molecular gas emission line widths and possible rotation curves (Frayer et al. 1998, 1999; Genzel et al. 2003; Neri et al. 2003). If we assume only the current maximum projected separations for the submillimeter galaxies (Fig. 3) and enclosed dynamical masses of order $\sim 5 \times 10^{11}\ M_{\odot}$, we can use Kepler's third law to calculate relaxation timescales. The median relaxation time is 30 Myr, with an interquartile range of 31 Myr. Hydrodynamic models have shown that supernovae may drive out the dust more easily than the gas in lower mass star-forming galaxies (Mac Low & Ferrara 1998). LBGs may be longer lived and lower mass galaxies that expelled the bulk of their dust prior to experiencing a luminous event of the submillimeter galaxy class.

In an accompanying paper, Conselice et al. (2003a) demonstrate that up to 80% of the submillimeter galaxies have morphologies consistent with major mergers. However, the radio emission typically points us to a single optical source, and only in the case of SMM J141809.8 (Chapman et al. 2002b) do we have spectroscopic confirmation that three components lie at the same redshift ($z = 2.99$). In addition, high-redshift galaxies often have complex morphologies (e.g., Cowie et al. 1995), and many appear qualitatively similar to the extended knotty structures shown in Figure 2 (although we have already considered in detail the LBG and NB galaxy morphologies, finding smaller and less disturbed configurations than the submillimeter galaxies). Alternative explanations to mergers have been presented in the literature. They could be associated with planar structures in the galaxy formation process, or they could be structures generated by sequential star formation (Cowie et al. 1995).

Can we decide whether an apparent clump of components, seen in many of our sources in Figure 2, is truly a merger versus an assembly of H II regions in a large galaxy? We previously showed how SMM J141809.8 displays a striking difference between its rest-frame UV and visible emission, a *morphological K-correction*, which is seen only rarely in more local galaxies (Hibbard & Vacca 1997; Abraham et al. 1999; Kuchinski et al. 2001; Windhorst et al. 2002). However, the most infrared-luminous local galaxies often show different morphologies in rest-frame near-IR (Scoville et al. 2000; Dinh-V-Trung et al. 2001). We must question how morphological *K*-correction might affect our interpretation of the submillimeter galaxies. We must also address how much structure is being resolved out by *HST*, lost to surface brightness dimming at redshifts $z \gg 1$. A well-studied local ULIRG, Mrk 231 (Goldader et al. 2002), shows 75 kpc tidal tails (10″ at the submillimeter galaxy redshifts). While we expect to miss many such features from the strong surface brightness dimming effects at high-z, we note that many of the optical morphologies do exhibit signs of extension. Colley et al. (1996) first made the argument that faint clumps at the same z close on the sky may be part of a larger galaxy, most of the underlying part not being visible due to SB dimming [the knots are unresolved, so they only dim as $\propto (1+z)^2$]. Without redshifts and velocity information for individual components, we cannot claim any source is a merger in progress. However, if it is not a merger yet, then it will likely be a future merger when the pieces come together and violently relax (barring the unlikely situation that σ_v is large enough for the violent relaxation to never happen). Regardless of the interpretation, these objects are clearly star formation wrecks of some sort, consistent with the submillimeter excess and plausibly young ages.

6. CONCLUSIONS

The *HST*-STIS images of submillimeter galaxies have clearly identified many large, distorted, and plausibly multiple component, merger systems. The physical separations of components are larger than similar luminosity *IRAS* galaxies seen locally, suggesting that they may typically represent an earlier stage of the merger process. The faint [$R'(573) > 24$] submillimeter sources on average have a larger effective radius (R_{50}) than the general "field" sample defined within the same STIS images. They are also typically larger than the $z \sim 3$ LBG population, defined in terms of R_{50} or Petrosian radius. The rest-frame UV extents and far-infrared estimated SFRs of these submillimeter galaxies are consistent with predictions based on the *maximal* star formation rate density of 20 $M_{\odot}$ kpc^{-2} seen in local starburst galaxies.

Consideration of the field sources with comparable R_{50} values often reveals highly elongated and distorted systems, some indistinguishable from the morphologies represented by the submillimeter galaxies. Scaling by the source count of the submillimeter galaxies at greater than 5 mJy (0.25 arcmin^{-2}) suggests that there are roughly 4 times the number of field galaxies with similar magnitudes and morphologies to the submillimeter galaxies that do not obviously generate the copious bolometric luminosities (they are undetected in the submillimeter and radio images). Our analysis of the LBGs and NB galaxies suggests that some of these field sources with morphologies similar to submillimeter galaxies would be LBGs/NB galaxies. It remains to be seen whether the bolometric luminosities and SFRs of the largest, irregular galaxies in the field are generally larger than the other field galaxy populations.

We would like to thank Ian Smail and Andrew Blain for detailed suggestions and comments on the manuscript that greatly helped improve the paper. We also acknowledge the detailed suggestions of an anonymous referee. This work is based on observations made with the NASA/ESA *Hubble Space Telescope*, obtained (from the Data Archive) at the Space Telescope Science Institute, which is operated by the Association of Universities for Research in Astronomy, Inc., under NASA contract NAS 5-26555. These observations are associated with proposal 9174. Support for proposal 9174 (S. C. C. and R. W.) was provided by NASA through a grant from the Space Telescope Science Institute.

APPENDIX A

Notes on Individual Objects

SMM J123553.3+621338.—A very extended galaxy with as many as 10 compact components arranged in a north-south assembly within 3.″4. Submillimeter flux (Chapman et al. 2001a), radio flux (Richards 2000).

SMM J123600.1+620254.—Five knots along a curve indicate that this galaxy is possibly an edge-on merger. Submillimeter flux (Chapman et al. 2001a), radio flux (Richards 2000).

SMM J123616.2+621514.—A trio of components suggest a system about to merge. To within the astrometric error, the brightest component appears to be aligned with the radio emission, a *Chandra* X-ray source (both hard and soft bands), and a *K*-band peak in the ground based (0.″5) image. Submillimeter flux (Chapman et al. 2001a), radio flux (Richards 2000).

SMM J123618.3+621551.—While only the central source is radio identified, the additional clumps lying within 2″ are plausibly associated, suggesting an early stage merger. Submillimeter flux (Barger et al. 2000), radio flux (Richards 2000).

SMM J123621.3+621708.—A strong radio peak with an extremely faint optical identification lies offset 2″ from a weaker radio peak associated with a north-south linear structure. Submillimeter flux (Barger et al. 2000), radio flux (Richards 2000).

SMM J123622.7+621630.—The radio centroid sits in a saddle of low surface brightness emission among a spectacular edge-on merger exhibiting five brightness peaks within an extended linear structure. The source is detected by *Chandra* in the hard X-ray band but not in the soft band. Submillimeter flux (Barger et al. 2000), radio flux (Richards 2000).

SMM J123710.0+622649.—This source has two radio sources lying within the SCUBA beam. The western source corresponds to a bright elliptical galaxy, the redshift of which is unknown. A photometric redshift from the available multiband imaging (B, V, I, K) suggests a $z \sim 0.4$ galaxy. There is no significant optical emission at the location of the eastern radio source. Submillimeter flux (Chapman et al. 2001a), radio flux (Richards 2000).

SMM J123713.9+621827.—The radio peak is offset by 0.″7 from an isolated and compact optical source, showing some extent in the northeast. This source is a bright *Chandra* X-ray source and is the strongest submillimeter emitter in our sample (16 mJy). With a radio flux of 595 mJy, it is also the strongest radio emitter. This source is likely to be a heavily dust obscured AGN. Submillimeter flux (Chapman et al. 2001a), radio flux (Richards 2000).

SMM J131231.9+424430.—A double extended source, with signs of low surface brightness features. This galaxy was detected at 6.7 μm using the *ISO* satellite by Sato et al. (2002), suggesting that many of these submillimeter galaxies will be routinely detected by the *SIRTF* mission. Submillimeter flux (Barger et al. 1999), radio flux (E. Richards 2003, private communication).

SMM J131235.2+424424.—This object is almost undetected, with only a faint 1.9 σ peak rising above the noise at the radio position (omitted from Fig. 2). As the source was detected at $I = 26.4$ in ground-based imagery, the *HST* may be resolving out a complex and diffuse structure. Submillimeter flux derived from our own reduction of the archival SCUBA data, radio flux (E. Richards 2003, private communication). The submillimeter and radio fluxes are presented in the figures of Chapman et al. (2002a).

SMM J141809.8+522205.—An assembly of bright blobs, with low surface brightness intervening material. A bridge of emission connects the strongest two components. Spectroscopic redshifts have been obtained for all three central blobs, $z = 2.99$ (Chapman et al. 2002b; see this work also for radio and submillimeter flux measurements). The original radio data in this region were presented in Fomalont et al. (1991). The UV spectroscopic redshift for the brightest *R*-band component is presented in Chapman et al. (2000). A strong *K*-band source lines up with northernmost blob, coincident with a millimeter interferometry measurement.

SMM J221724.7+001242.—A filamentary object, which appears like an irregular edge-on galaxy, flanked by two compact components. The galaxy is identified in the Very Large Array B-array radio map and in the archival *Chandra* X-ray image. Lensing from the bright galaxy to the northwest may be subtly distorting the image (Chapman et al. 2002c). Fitting and subtracting the bright elliptical galaxy does not reveal any additional structure or components. The updated radio and submillimeter fluxes for this source are presented in S. C. Chapman et al. 2004 (in preparation).

SMM J221726.1+001239.—This is the "blob 1" submillimeter source (Steidel et al. 2000; Chapman et al. 2001a) lying at the center of a $z = 3.09$ protocluster. The *HST* image reveals a faint, apparently linear system, with surrounding, very faint components that could represent a merger in progress. A brighter unresolved core along the linear structure suggests an AGN or a more concentrated starburst. While no significant radio emission has been detected to isolate the position of the submillimeter source, an interferometric detection of molecular gas in CO (4–3) identifies the submillimeter emission with this *HST* source (Chapman et al. 2003b). The radio and submillimeter fluxes and the spectroscopic redshift for this source are also detailed in Chapman et al. (2003b).

REFERENCES

Abraham, R. G., Ellis, R. S., Fabian, A. C., Tanvir, N. R., & Glazebrook, K. 1999, MNRAS, 303, 641
Alexander, D., et al. 2003, AJ, 125, 383
Barger, A. J., Cowie, L. L., & Richards, E. A. 2000, AJ, 119, 2092
Barger, A. J., Cowie, L. L., & Sanders, D. B. 1999, ApJ, 518, L5
Bershady, M., Jangren, A., & Conselice, C. 2000, AJ, 119, 2645
Bertin, A., & Arnouts, S. 1996, A&AS, 117, 393
Blain, A. W., Chapman, S. C., Smail, I., & Ivison, R., 2003, ApJ, submitted
Blain, A. W., Smail, I., Ivison, R. J., & Kneib, J.-P. 1999, MNRAS, 302, 632
Capak, P., et al. 2003, ApJ, in press
Carilli, C. L., & Yun, M. S. 1999, ApJ, 513, L13
———. 2000, ApJ, 539, 1024
Chapman, S. C., Blain, A., Ivison, R., & Smail, I. 2003a, Nature, 422, 695
Chapman, S. C., Lewis, G., Scott, D., Borys, C., & Richards, E. 2002a, ApJ, 570, 557
Chapman, S. C., Richards, E. A., Lewis, G. F., Wilson, G., & Barger, A. J. 2001a, ApJ, 551, L9
Chapman, S. C., Scott, D., Windhorst, R., Frayer, D., Borys, C., & Lewis, G. 2003b, ApJ, submitted
Chapman, S. C., Shapley, A., Steidel, C., & Windhorst, R. 2002b, ApJ, 572, L1
Chapman, S. C., Smail, I., Ivison, R., & Blain, A. 2002c, MNRAS, 335, L17
Chapman, S. C., et al. 2000, MNRAS, 319, 318

Chapman, S. C., et al. 2001b, ApJ, 548, L17
———. 2003c, ApJ, 585, 57
Colley, W., Rhoads, J., Ostriker, J., & Spergel, D. 1996, ApJ, 473, L63
Condon, J. J. 1992, ARA&A, 30, 575
Conselice, C. J. 2003, ApJS, 147, 1
Conselice, C. J., Bershady, M. A., & Gallagher, J. S. 2000, A&A, 354, L21
Conselice, C., Bershady, M., & Jangren, A. 2000, ApJ, 529, 886
Conselice, C. J., Chapman, S., & Windhorst, R. 2003a, ApJL, in press
Conselice, C. J., et al. 2003b, AJ, 126, 1183
Cowie, L., & Hu, E. 1998, AJ, 115, 1319
Cowie, L., Hu, E., & Songaila, A. 1995, AJ, 110, 1576
Dinh-V-Trung, K., et al. 2001, ApJ, 556, 141
Erb, D., et al. 2003, ApJ, 591, 101
Farrah, D., Verma, A., Oliver, S., Rowan-Robinson, M., & McMahon, R. 2002, MNRAS, 329, 605
Fomalont, E., Windhorst, R., Kristian, J., & Kellerman, K. 1991, AJ, 102, 1258
Frayer, D., et al. 1998, ApJ, 506, L7
———. 1999, ApJ, 514, L13
Genzel, R., et al. 2003, ApJ, 584, 633
Giavalisco, M., Steidel, C., & Machetto, D. 1996, ApJ, 470, 189
Goldader, J., Meurer, G., Heckman, T., Seibert, M., Sanders, D., Calzetti, D., & Steidel, C. 2002, ApJ, 568, 651
Graham, A., Erwin, P., Caon, N., & Trujillo, I. 2001, ApJ, 563, 11
Helou, P., et al. 1985, ApJ, 440, 35
Hibbard, J. E., & Vacca, W. D. 1997, AJ, 114, 1741
Ivison, R., Smail, I., Frayer, D., Kneib, J.-P., & Blain, A. W. 2001, ApJ, 561, L45
Ivison, R. et al. 2002, MNRAS, 337, 1
Kim, D., et al. 1998, ApJ, 508, 627
Kim, D., & Sanders, D. B. 1998, ApJS, 119, 41
Kuchinski, L. E., Madore, B. F., Freedman, W. L., & Trewhella, M. 2001, AJ, 122, 729
Lehnert, M., & Heckman, T. 1996, ApJ, 472, 546
Lilly, S., et al. 1999, ApJ, 518, 641
Mac Low, M.-M., & Ferrara, A. 1998, in IAU Colloq. 166, The Local Bubble and Beyond, ed. D. Breitschwerdt, M. J. Freyberg, & J. Trümper (Berlin: Springer), 559
Mihos, C., & Bothun, G. 1998, ApJ, 500, 619
Mihos, C., & Hernquist, L. 1996, ApJ, 464, 641
Murphy, T., et al. 1996, AJ, 111, 1025
Neri, R., et al. 2003, preprint (astro-ph/0307310)
Odewahn, S. C., Cohen, S. H., Windhorst, R. A., & Philip, N. S. 2002, ApJ, 568, 539
Richards, E. A. 2000, ApJ, 533, 611
Richards, E. A., et al. 1999, ApJ, 526, L73
Sanders, D., & Mirabel, F. 1996, ARA&A, 34, 749
Sato, Y., Cowie, L. L., Kawara, K., Taniguchi, Y., Sofue, Y., Matsuhara, H., & Okuda, H. 2002, ApJ, 578, L23
Scoville, N., et al. 2000, AJ, 119, 991
Smail, I., Ivison, R. J., & Blain, A. W. 1997, ApJ, 490, L5
Smail, I., Ivison, R. J., Blain, A. W., & Kneib, J.-P. 1998, ApJ, 507, L21
———. 2002, MNRAS, 331, 495
Steidel, C., Adelberger, K., Dickinson, M., Giavalisco, M., Pettini, M., & Kellogg, M. 1998, ApJ, 492, 428
Steidel, C., Adelberger, K., Giavalisco, M., Dickinson, M., & Pettini, M. 1999, ApJ, 519, 1
Steidel, C., Giavalisco, M., Dickinson, M., & Adelberger, K. 1996, AJ, 112, 352
Steidel, C., et al. 2000, ApJ, 532, 170
———. 2003, ApJ, in press
Surace, J., & Sanders, D. 2000, AJ, 120, 604
Tacconi, L., et al. 2002, ApJ, 580, 73
Veilleux, S., Kim, D., & Sanders, D. 2002, ApJS, 143, 315
Windhorst, R. A., et al. 1995, Nature, 375, 471
———. 2002, ApJS, 143, 113